Desalination and Water Treatment
www.deswater.com

doi: 10.1080/19443994.2015.1064033

57 (2016) 14622–14631
July

Taylor & Francis
Taylor & Francis Group

Rapid photo- and photo-Fenton-like catalytic removals of malachite green in aqueous solution on undoped and doped TiO_2 nanotubes

H.-Y. He*, C.-Y. Tian

College of Materials Science and Engineering, Shaanxi University of Science and Technology, Xi'an 710021, China, Tel. +86 15319453608; email: 917894940@qq.com, hehy@sust.edu.cn (H.-Y. He), Tel. +86 12256677889; email: 476946195@qq.com (C.-Y. Tian)

Received 11 February 2015; Accepted 14 June 2015

ABSTRACT

Undoped and Fe-doped TiO_2 nanotubes with Fe content of 0–3.86 at.% were fabricated by hydrothermally treating sol–gel-derived undoped and Fe-doped TiO_2 nanoparticles in NaOH aqueous solution. The Fe doping narrowed the optical band gap of the nanotubes from 3.17 to ~2.76 eV as the increase in Fe-doping content from 0 to 3.86 at.%. The nanotubes showed a large specific surface area of ~274–303 $m^2 g^{-1}$, which increased as the increase of Fe content. The sunlight-excited degradation experiments of malachite green in the water indicated that the nanotubes had a high photocatalytic activity. The Fe doping further enhanced the photocatalytic activity of the nanotubes, increased as increasing Fe-doping content. Moreover, the photodegradation of the dye became more fast as H_2O_2 was used, showing remarkable Fenton-like photocatalytic activity. This Fenton-like reaction also enhanced as increasing Fe content. An optimal H_2O_2 dosage was also observed. The quasi-kinetic first-order rate constant of the photodegradation of the malachite green aqueous solution with the concentrations of 1×10^{-6} and 1×10^{-5} mol l^{-1} were in the range of ~1.61–2.03 and ~0.41–0.65 min^{-1}, respectively. These constants further increased to ~2.81–3.51 and ~1.71–2.04 min^{-1} as the H_2O_2 with a concentration of 10 ml l^{-1} is used.

Keywords: Semiconductors; Nanotubes; Photocatalytic properties; Fenton-like reaction

1. Introduction

Nano-TiO_2 materials as a photocatalyst have been widely studied for potential application in decontamination of environmental pollutants. Photocatalytic property of TiO_2 nanomaterials is intimately dependent on light absorption. However, TiO_2 is only activated in the ultraviolet region, which restricted its application in nature light condition. Therefore, a large number of efforts were made to enhance the light absorption for improving the photocatalytic property of the TiO_2. Doping nitrogen [1,2], sulfur [2,3], and some metal cations [4,5] were usually used to narrow the bandgap of TiO_2. The Fe doping has been verified to be more effective than other metal cations [5,6], and thereby being widely studied [4–10].

The photocatalytic activity of the Fe-doped TiO_2 nanomaterials is also associated with their morphology. Nanotubes are of great interest due to their high surface-to-volume ratios. Several recent studies have indicated that TiO_2 nanotubes have improved properties when compared to any other form of TiO_2 as used

*Corresponding author.

as photocatalyts [11,12]. TiO_2 nanotubes and nanotube arrays have been produced by a variety of methods. These methods include using the nanoporous alumina as template [13], sol–gel transcription using organogelators as templates [14,15], seeded growth [16], hydrothermal processes [17–19], and anodization route [20–23]. However, the fabrication and photocatalysis of Fe-doped TiO_2 nanotubes is rarely reported in the previous literature.

Malachite green as an alkaline green dye usually exists in the wastewater produced from printing and dyeing processes in silk, leather, and paper industry. This dye is noxious to human and environment, and so must be removed before discharging the wastewater into environment.

In this work, we focus on (i) the fabrication of undoped and Fe-doped TiO_2 nanoparticles and nanotubes, (ii) the effect of Fe-doping level on the photocatalytic activity of TiO_2 nanotubes in the photodegradation of malachite green in the water, and (iii) the photo-Fenton-like reaction on the nanotubes in the degradation of malachite green in the water.

2. Experimental section

The undoped and doped TiO_2 nanoparticles (NPs) with different Fe contents were synthesized by a sol–gel process. First, butyl titanate ($C1_6H_{36}O_4Ti$) was dissolved in ethanol. Into such solution, ferric nitrate ($Fe(NO_3)_3{\cdot}9H_2O$) was then dissolved to prepare precursor solutions with molar ratios of Fe/Ti = 1, 2, and 3 at.%, respectively. Citric acid about 1.5 times molar of the metal cations, as a chelating agent, was added into the solutions with and without Fe cation. The solutions were then stabilized with a little acetylacetone (~1 ml) and then expanded to 100 ml with ethanol. The transparent solutions with Ti cation concentration of 0.1 mol l^{-1} were formed after constant stirring for 30 min. The gel solutions were dried at 80°C for 12 h and then 150°C for 7 h. As-dried gels were calcined at 400°C for 2 h in air. The undoped and Fe-doped TiO_2 nanotubes (NTs) were fabricated by hydrothermally treating the above prepared nanoparticles in 10 mol l^{-1} of NaOH aqueous solution at 110°C for 24 h, as used in the previous literature [17,18]. The products were filtered, washed repeatedly with deionic water until washing liquid near neutral, and then dried at 80°C for 3 h. Finally, the products were crystallized at 400°C for 1 h. The color of the products changed from white to yellow as the increase in Fe content.

The phases of the nanoparticles and nanotubes were identified at room temperature using a X-ray diffractometer (XRD, Cu Kα1, λ = 0.15406 nm, Model No: D/Max-2200PC, Rigaku, Japan). The morphology and X-ray energy dispersive spectra (EDS) of the nanotubes were analyzed using a transmission electron microscopy (TEM, Model No: JEM-3010, Japan). The diffusion–reflection absorption spectra of the nanotubes on a UV–vis spectrophotometer (Model No: Lambda 950, Bruker Daltonics, USA) were in the range of 200–800 nm. Specific surface area of the nanoparticles and nanotubes were measured by N_2 absorption method on a surface area analyzers (Model no: Autosorb-6iSA, Quantachrome Instruments, US).

Malachite green dye was used as a photocatalytic substrate to study the photocatalysis of the nanotubes in this study. The photocatalysis experiments were performed in a glass beaker at a temperature of ~25°C. The malachite green aqueous solutions with two concentrations of 1×10^{-6} and 1×10^{-5} mol l^{-1} were first prepared. In each experiment, 50-mg nanotubes and 50-ml malachite green aqueous solution were added to a glass breaker. At the same time, in such two other systems, the H_2O_2 was added to make its concentration equals 10 and 20 ml l^{-1}. The artificial sunlight with the illumination intensities of ~25 and ~500 W m^{-2} were used as light sources for the photodegradation of the malachite green aqueous solutions with the concentrations of 1×10^{-6} and 1×10^{-5} mol l^{-1}, respectively. After different irradiation times, ~3-ml solution was took out and filtrated out the suspended tiny particles and subsequently measured for their light absorbance at ~617 nm on a spectrophotometer (Model No: 752N, China). The solution after the test was returned to the breaker to maintain the normal volume of the solution under the test.

In the period of first hour of the above photocatalytic experiments, the oxidation–reduction potentials of the malachite green aqueous solutions with and without the nanotubes were measured on an oxidation–reduction potential tester (ORP-286, China). Their difference was used as a determination of the oxidation–reduction potentials of the nanotubes surface.

The quasi-kinetic first-order rate constant (k_1) were calculated with the kinetic relation between the concentration (C) of the malachite green aqueous solution and the first photocatalytic reaction span (t) given by:

$$\frac{C_0}{C} = \mathrm{A}\ \exp\left(\frac{k_1 t}{T}\right) \tag{1}$$

In which, C_0 and C are the initial concentration and concentration of the dye aqueous solution, respectively, T is reaction temperature, and A is a constant.

3. Results and discussion

3.1. Microstructure and phase of the nanoparticles and nanotubes

Figs. 1a and 1b show the XRD pattern of the synthesized nanoparticles and nanotubes. The XRD peaks of the nanoparticles correspond to the two phases of anatase and rutile (Fig. 1a). The initial nanotubes are amorphous and transferred to anatase and rutile after the crystallization (Fig. 1b). The average crystallite sizes of the nanoparticles and nanotubes are estimated with Scherrer's equation,

$$D = 0.9\frac{\lambda}{\beta \cos \theta} \quad (2)$$

The results are shown in Fig. 1c. They are decreased overall with the increase in Fe-doping content. This can be ascribed to the inhibition of Fe^{3+} cation in the TiO_2 crystal growth because of its different cation ratio (0.64 Å) with Ti^{4+} cation (0.68 Å). The small difference in the particle sizes of the nanoparticles and nanotubes could mainly come from the polycrystalline characteristics of the nanoparticles. The interplanar placings of main lattice planes of the nanotubes are listed in Table 1 and are smaller than the value reported in JSPDS card. The smaller lattice parameters of the nanotubes could be ascribed to high crystallinity and small ratio of Fe^{3+} cation than Ti^{4+} cation.

Figs. 2a–2d illustrate the TEM micrographs of the undoped and Fe-doped TiO_2 nanotubes. All the nanotubes show very small pore size and multi-channel morphology. The EDS analyses of the nanotubes

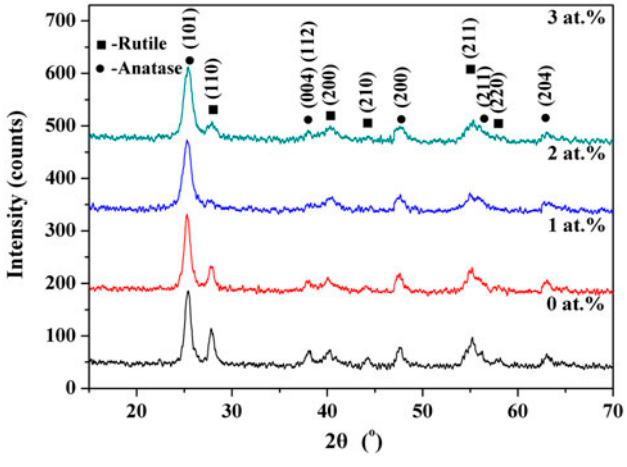

Fig. 1a. XRD pattern of the pure and Fe-doped TiO_2 nanoparticles.

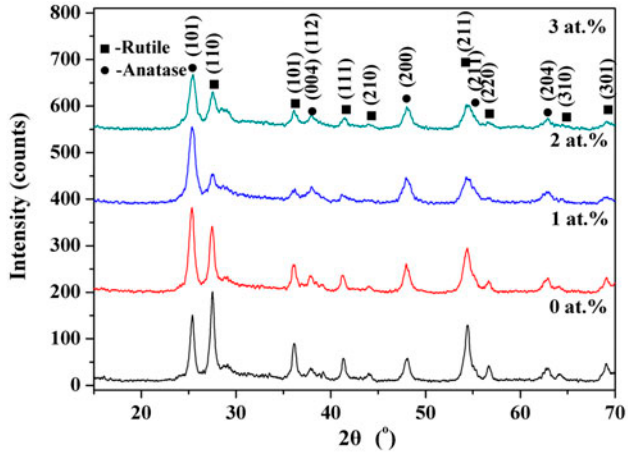

Fig. 1b. XRD pattern of the pure and Fe-doped TiO_2 nanotubes.

(Figs. 3a–3d) reveal that their Fe/Ti ratio are ~0 and ~1.26, ~2.58 and ~3.86 at.%, respectively. These ratios are larger than that in their precursor solutions. This could reveal that Ti cations were etched out faster than Fe cation in the hydrothermal process in NaOH aqueous solution.

3.2. Specific surface area analysis of the nanoparticles and nanotubes

The BET surface area (S_{BET}) of the undoped and doped TiO_2 nanoparticles and nanotubes were measured by nitrogen absorption method. The S_{BET} of the nanotubes with the Fe contents of 0, 1.26, 2.58, and 3.86 at.% were ~274, ~311, ~316, and ~303 $m^2\ g^{-1}$,

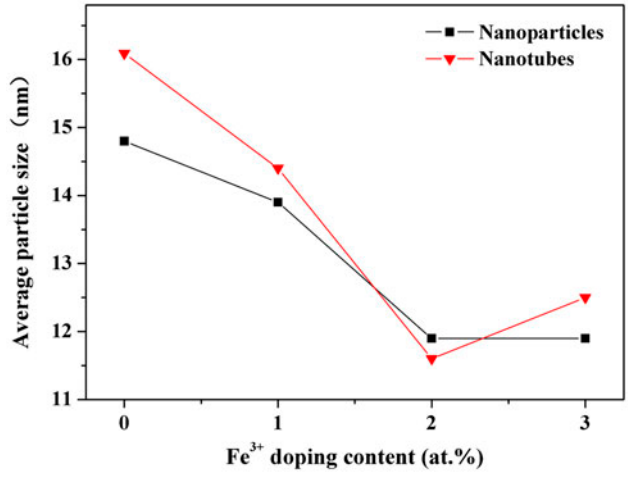

Fig. 1c. Average particle size of the nanoparticles and nanotubes determined from XRD data analysis.

Table 1
Interplanar spacing of main lattice plane of the Fe-doped TiO_2 nanotubes fabricated from the precursor solution with different Fe-doping contents

Phase	Lattice plane	*d* (Å)					
		0 at.%	1 at.%	2 at.%	3 at.%	76-1938[a]	73-1764[b]
Rutile	110	3.2385	3.2431		3.2384	3.2477	
Rutile	101	2.4820	2.4820	2.4793	2.4794	2.4875	
Rutile	111	2.1812	2.1813	2.1853	2.1832	2.1873	
Rutile	301	1.3576	1.3576	1.3575	1.3569	1.3598	
Anatase	101	3.5038	3.5009	3.5065	3.4930		3.5083
Anatase	200	1.8880	1.8864	1.8879	1.8864		1.8880

[a]JSPDS card no. of the rutile.
[b]JSPDS card no. of the anatase.

Table 2
The quasi-kinetic first-order rate constants k_1 (min^{-1}) in the conditions of various concentrations of the H_2O_2 ($C_{H_2O_2}$) and malachite green (C_{MG}), and different sunlight intensities (*I*)

Fe content (at.%)	C_{MG} (mol l^{-1})	*I* (W m^{-1})	$C_{H_2O_2}$ (mol l^{-1})		
			10	20	20
0	1×10^{-6}	25	1.61	2.81	2.66
1.26	1×10^{-6}	25	1.77	3.00	2.90
2.58	1×10^{-6}	25	2.04	3.22	3.07
3.86	1×10^{-6}	25	2.30	3.51	3.35
0	1×10^{-5}	500	0.41	1.71	0.94
1.26	1×10^{-5}	500	0.54	1.80	0.99
2.58	1×10^{-5}	500	0.60	1.90	1.14
3.86	1×10^{-5}	500	0.65	2.04	1.39

respectively. These values are obviously larger than that of the nanoparticles (~41–52 m^2 g^{-1}).

3.3. Optical absorption of the undoped and Fe-doped TiO_2 nanotubes

Figs. 4a and 4b show the UV–visible diffuse reflective absorption spectra of the nanotubes. The light absorption extends to visible region as increasing Fe content. The absorption edge (λ_e) of the nanotubes with Fe content of 0, 1.26, 2.58, 3.86 at.% are ~396, ~418, ~431, and ~449 nm, respectively. Correspondingly, the bandgap energies (E_g) are ~3.14, ~2.97, ~2.88, and ~2.76 eV, respectively, according to the relation of $E_g = 1{,}240/\lambda_e$. Such large variation due to small amount of Fe doping could be ascribed to the introduction of the impurity level into the TiO_2. The schematic diagram of energy levels and initial redox process of the Fe-doped TiO_2 nanotubes in the process of sunlight excitation can be proposed in Fig. 5 on basis of the method reported in the previous literature [7,24,25].

3.4. Photocatalysis of the undoped and Fe-doped TiO_2 nanotubes

Figs. 6a–6c and 7a–7c show the concentration variations of the malachite green aqueous solutions with the dye concentration of 1×10^{-6} and 1×10^{-5} mol/l on the nanotubes with the irradiation times in the sunlight. The quasi-kinetic first-order rate constants k_1 are listed in Table 2. The degradation rates and k_1 increase as the increase in Fe-doping content. This is agreed to the increase in light absorption, which could indicate that the light-generated electron–hole pairs play a main role in the photocatalytic degradation. In addition, all k_1 values have become smaller after first photocatalytic reaction span, which could be ascribed to that the dye absorption on the nanotubes surface mainly take place in the first span.

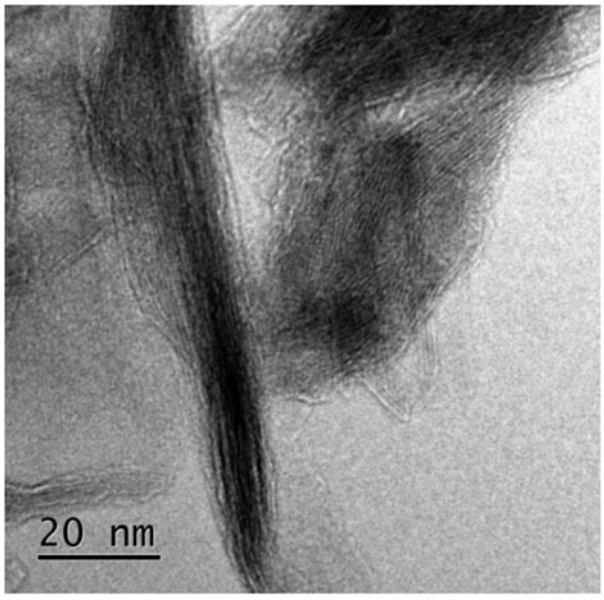

Fig. 2a. TEM micrographs of the pure TiO_2 nanotubes.

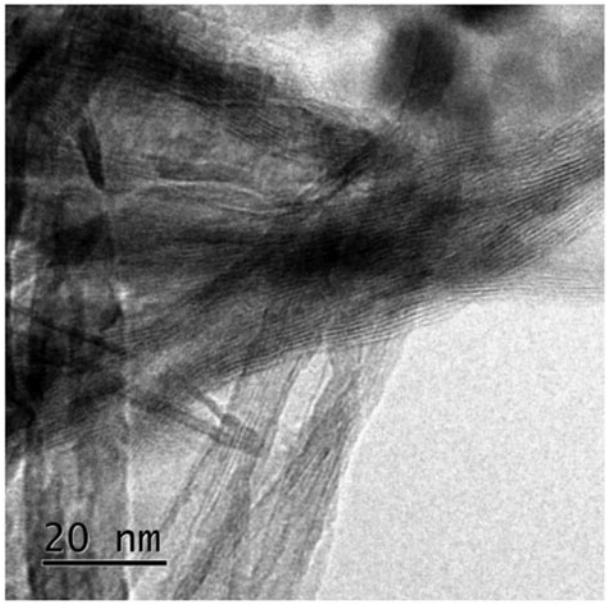

Fig. 2b. TEM micrographs of the Fe-doped TiO_2 nanotubes fabricated from the precursor solution with the Fe content of 1 at.%.

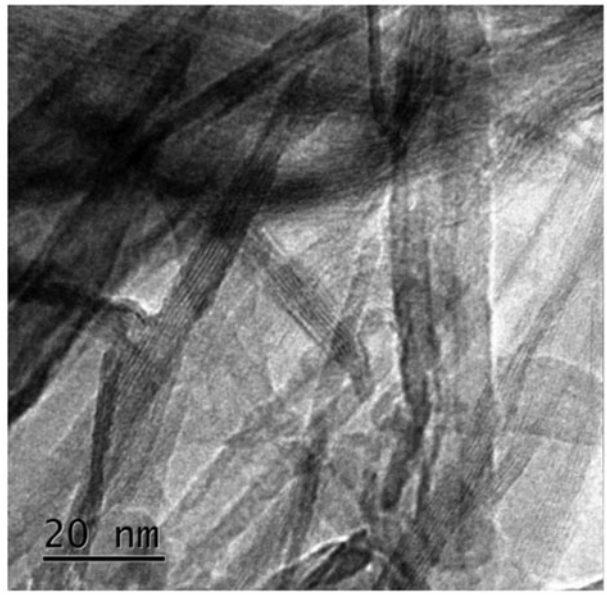

Fig. 2c. TEM micrographs of the Fe-doped TiO_2 nanotubes fabricated from the precursor solution with the Fe content of 2 at.%.

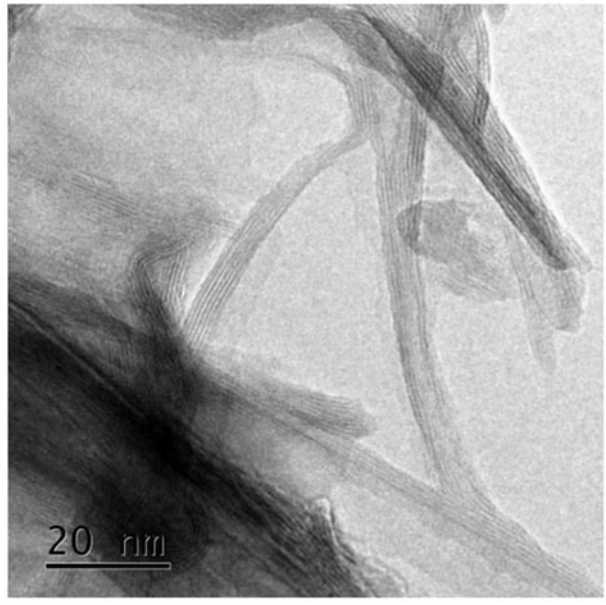

Fig. 2d. TEM micrographs of the Fe-doped TiO_2 nanotubes fabricated from the precursor solution with the Fe content of 2 at.%.

In recent years, advanced oxidation processes using UV/H_2O_2 have become a way to degrade organic compounds in dilute solutions. In general, it is believed that the UV/H_2O_2 processes can result in the formation of OH radicals in the solution, which can accelerate the degradation of the organic compounds in water. The combined use of H_2O_2 and semiconductors under light irradiation, a well-known Fenton-like process, is an efficient way of further enhancing photodegradation rate. In the photodegradation of the malachite green in

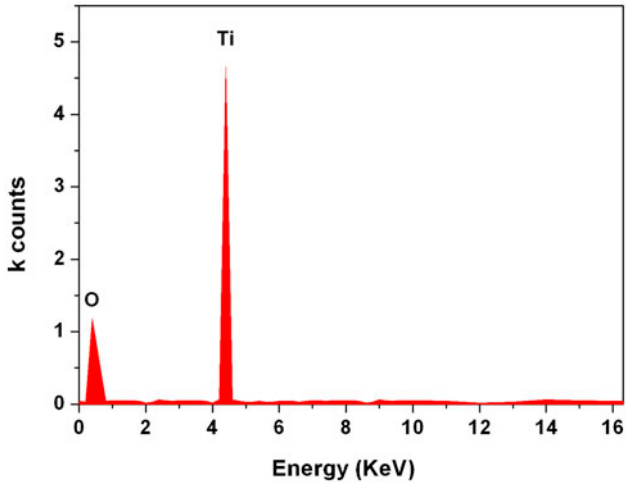

Fig. 3a. EDS of the pure TiO_2 nanotubes.

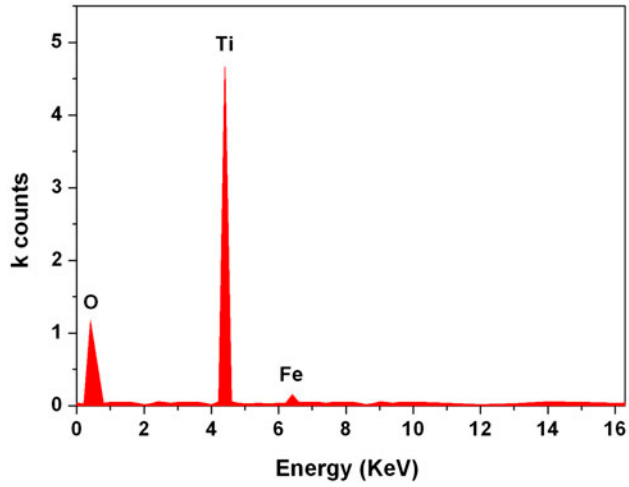

Fig. 3c. EDS of the Fe-doped TiO_2 nanotubes fabricated from the precursor solution with Fe content of 2 at.%.

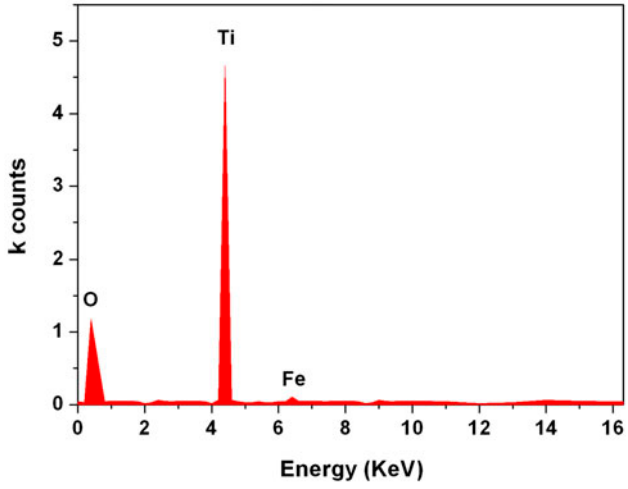

Fig. 3b. EDS of the Fe-doped TiO_2 nanotubes fabricated from the precursor solution with Fe content of 1 at.%.

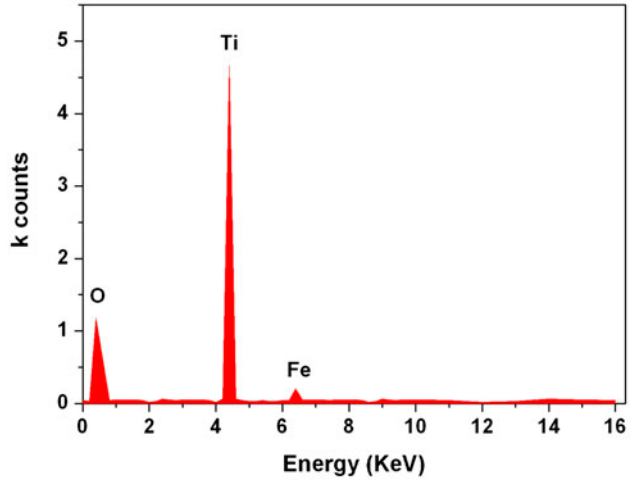

Fig. 3d. EDS of the Fe-doped TiO_2 nanotubes fabricated from the precursor solution with Fe content of 3 at.%.

the water on the nanotubes, the H_2O_2 obviously speeds up the photodegradation process (Figs. 6a–6c and 7a–7c), showing a photo-Fenton-like reaction. The H_2O_2 of 10 ml/l shows the best effect, further increasing H_2O_2 concentration to 20 ml/l leads to a slight decrease in the degradation rate. Similar feature of the best H_2O_2 concentration has also been reported by Elmolla and Chaudhuri [26], who believed that the H_2O_2 is considered to have two functions in the photocatalytic process. It accepts a photogenerated electron from the conduction band of the semiconductor to form ·OH radical (Reaction (3)). In addition, it forms ·OH radicals according to Reaction (4):

$$H_2O_2 + e^- \rightarrow {\cdot}OH + OH^- \quad (3)$$

$$H_2O_2 + {\cdot}O_2^- \rightarrow {\cdot}OH + OH^- + O_2 \quad (4)$$

The ·OH and OH^- radicals play an oxidation and reduction in the photodegradation process. However, excess H_2O_2 reacts with ·OH and contributes to the

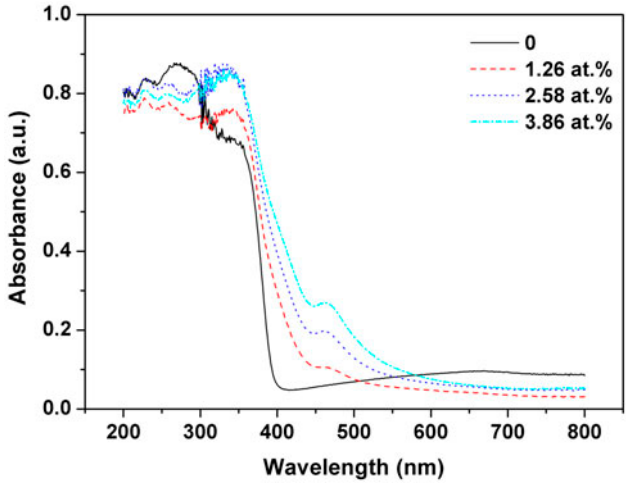

Fig. 4a. Adsorption spectra of the pure and Fe-doped TiO_2 nanotubes.

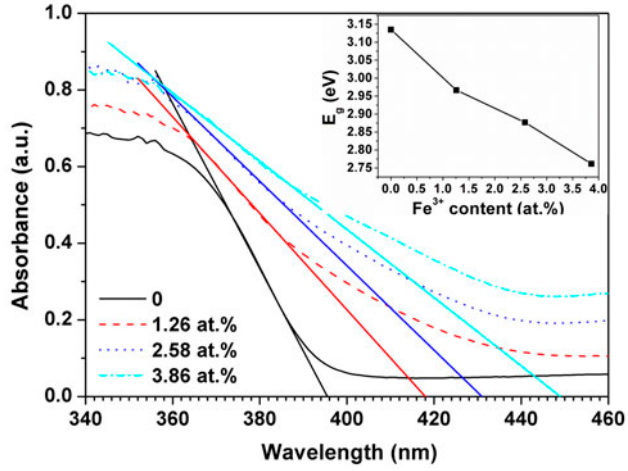

Fig. 4b. Enlarged figure of absorbance spectra of the nanotubes in 340–360 nm. Inserted figure is the variation of bandgap with Fe content.

·OH and hole scavenging to form $HO_2^{\cdot}$ as in Reactions (5) and (6).

$$\cdot OH_2 + H_2O_2 \rightarrow H_2O + HO_2^{\cdot} \quad (5)$$

$$H_2O_2 + h^+ + \rightarrow H^+ + HO_2^{\cdot} \quad (6)$$

Therefore, it is necessary to choose the optimum concentration of H_2O_2 according to the type and concentration of the pollutants. Furthermore, the photo-Fenton-like degradation rate of the dye also increases as increasing Fe content. The photogenerated electrons and holes in the nanotubes could play the similar role of the Fe^{2+} and Fe^{3+} cations in Fenton reaction. The concentration increase of photogenerated electrons and holes as the increase in Fe content leads to the enhanced Fenton-like reaction in the dye degradation. In this view, the optimal H_2O_2 concentration could be also associated with the dosage of the photocatalyst.

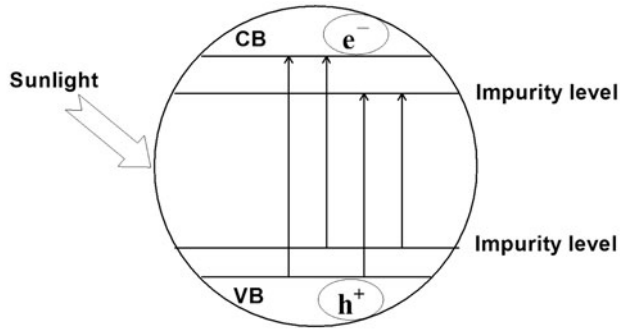

Fig. 5. Schematic diagram of energy level and initial redox process of the pure and Fe-doped TiO_2 nanotubes in the process of sunlight excitation.

The acidic–alkaline behavior of a photocatalyst surface is usually evaluated by oxidation–reduction potential [27–29]. The oxidation–reduction potential of the nanotubes in the photocatalysis system (ORP) was measured. The oxidation of H_2O_2 leads to an ORP increase of the photocatalysis system. However, this increase is smaller than that of the dye aqueous solution in the absence of the nanotubes. Thus, the measured ORP (Figs. 8a and 8b) has larger negative

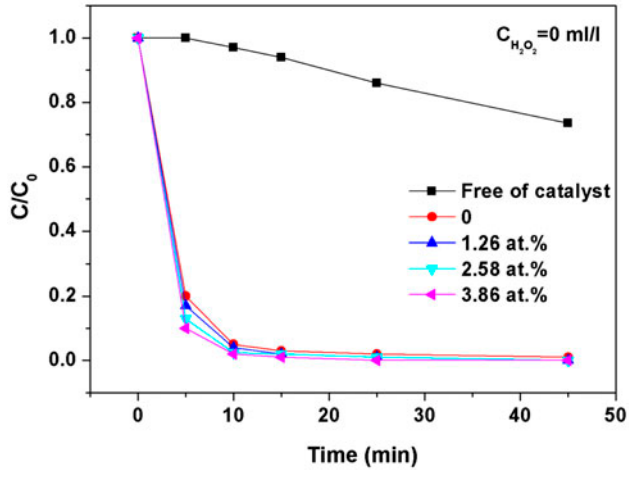

Fig. 6a. Concentration variations of malachite green aqueous solution with the concentration of 1×10^{-6} mol l^{-1} without H_2O_2 ($C_{H_2O_2} = 0$) on the pure and Fe-doped TiO_2 nanotubes with sunlight irradiation time (sunlight intensity = ~25 W m^{-2}).

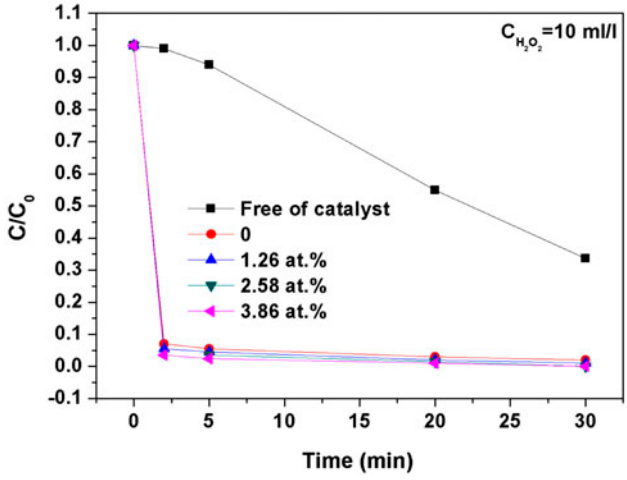

Fig. 6b. Concentration variations of malachite green aqueous solution with the concentration of 1×10^{-6} mol l^{-1} and H_2O_2 concentration $C_{H_2O_2}$ = 10 ml/l on the pure and Fe-doped TiO_2 nanotubes with sunlight irradiation time (sunlight intensity = ~25 W m^{-2}).

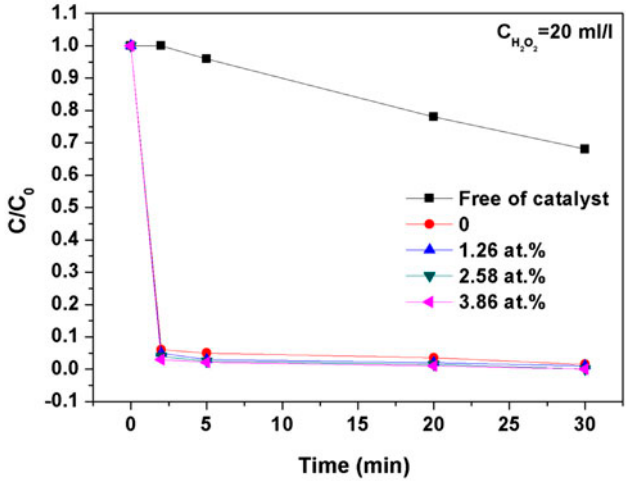

Fig. 6c. Concentration variations of malachite green aqueous solution with the concentration of 1×10^{-6} mol l^{-1} and H_2O_2 concentration $C_{H_2O_2}$ = 20 ml/l on the pure and Fe-doped TiO_2 nanotubes with sunlight irradiation time (sunlight intensity = ~25 W m^{-2}).

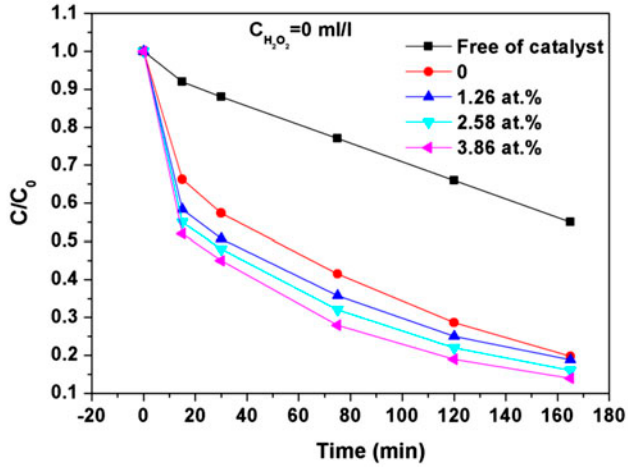

Fig. 7a. Concentration variations of malachite green aqueous solution with the concentration of 1×10^{-5} mol l^{-1} without H_2O_2 ($C_{H_2O_2}$ = 0) on the pure and Fe-doped TiO_2 nanotubes with sunlight irradiation time (sunlight intensity = ~500 W m^{-2}).

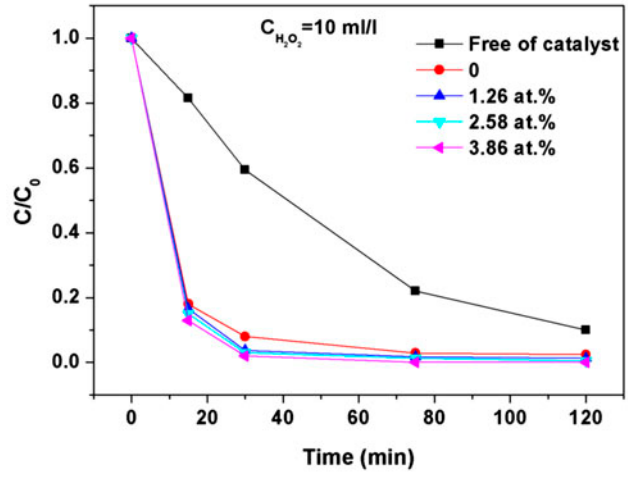

Fig. 7b. Concentration variations of malachite green aqueous solution with the concentration of 1×10^{-5} mol l^{-1} and H_2O_2 concentration $C_{H_2O_2}$ = 10 ml/l on the pure and Fe-doped TiO_2 nanotubes with sunlight irradiation time (sunlight intensity = ~500 W m^{-2}).

values. This implies that the reduction enhancement of photogenerated electrons is superior and the reduction is a dominant characterization of the nanotubes surface in the photocatalysis systems. Moreover, the ORP become more negative as increasing the Fe-doping content and using H_2O_2, implying the enhancement of the reduction characterizations of the nanotubes surface with Fe doping and using H_2O_2 in the sunlight. This is consistent with the variation of the photodegradation of the malachite green in the water with Fe content and using H_2O_2. Therefore, the photodegradation of dye is mainly reductive and

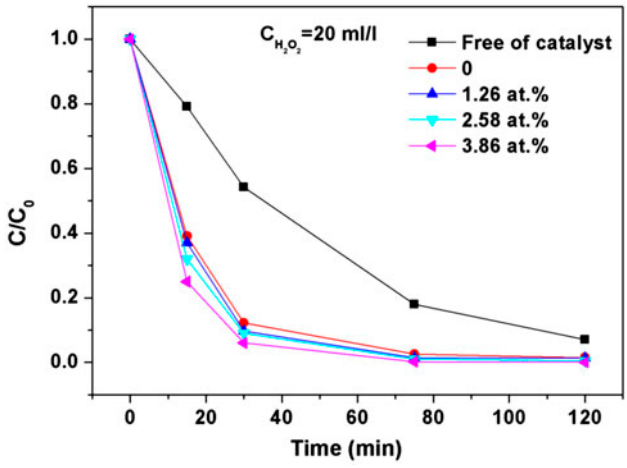

Fig. 7c. Concentration variations of malachite green aqueous solution with the concentration of 1×10^{-5} mol l^{-1} and H_2O_2 concentration $C_{H_2O_2}$ = 20 ml/l on the pure and Fe-doped TiO_2 nanotubes with sunlight irradiation time (sunlight intensity = ~500 W m^{-2}).

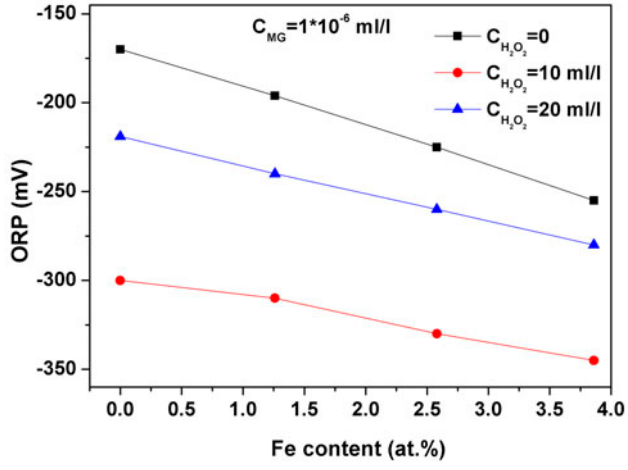

Fig. 8a. ORP variations of the nanotube surface with Fe content in the conditions of various H_2O_2 concentrations ($C_{H_2O_2}$), dye concentration of $C_{MG} = 1 \times 10^{-6}$ mol l^{-1}, and sunlight intensity = ~25 W m^{-2}.

the photogeneratged electrons play a dominant role in the photocatalytic degradation. The increase of photogenerated electrons and holes as the increase in Fe content leads to the further enhanced Fenton-like reaction in the dye degradation.

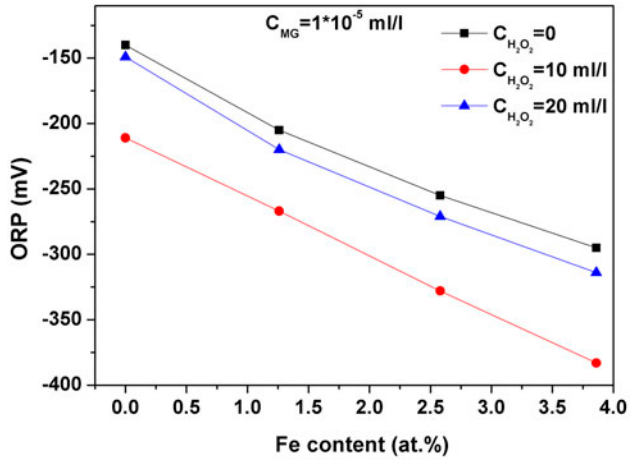

Fig. 8b. ORP variations of the nanotube surface with Fe content in the conditions of dye concentration of $C_{MG} = 1 \times 10^{-5}$ mol l^{-1}, various H_2O_2 concentrations ($C_{H_2O_2}$), and sunlight intensity = ~500 W m^{-2}.

4. Conclusion

Undoped and Fe-doped TiO_2 nanotubes with Fe content up to 3.86 at.% were prepared by a sol–gel route followed by hydrothermal treatment in NaOH aqueous solution and annealing crystallization. The Fe doping decreased the average particle size and extended absorbance edges to visible light region to ~449 nm (~2.76 eV) as Fe content equaled maximal value of 3.86 at.%. The nanotubes showed small pore size and multi-channel morphology. The specific surface area of the nanotubes is ~274–303 m^2 g^{-1} that increased as the increase in Fe content. These values are remarkably larger than that of the nanoparticles (~41–52 m^2 g^{-1}). Increasing Fe-doping content can obviously increase the photocatalytic activity of the nanotubes in the sunlight degradation of malachite green in the water. Significantly, small amount of H_2O_2 (10 ml l^{-1}) can obviously speed up the dye photodegradation rate. Large specific surface area and high photocatalytic activity make the Fe-doped TiO_2 nanotubes are promising photocatalytic nanomaterials for the application of environment purification.

The oxidation–reduction potential measurement indicated that the nanotubes surface showed a dominant reduction characterization that enhanced as the increase of Fe content and the utilization of H_2O_2. Thus, the nanotubes might be more suitable to photodegrade acidic organic pollution.

References

[1] T. Lindgren, J.M. Mwabora, E. Avendaño, J. Jonsson, A. Hoel, C. Granqvist, S. Lindquist, Photoelectrochemical and optical properties of nitrogen doped titanium dioxide films prepared by reactive DC magnetron sputtering, J. Phys. Chem. B 107 (2003) 5709–5716.

[2] K. Nishijima, B. Ohtani, X.-L. Yan, T.-A. Kamai, T. Chiyoya, T. Tsubota, N. Murakami, T. Ohno, Incident light dependence for photocatalytic degradation of acetaldehyde and acetic acid on S-doped and N-doped TiO_2 photocatalysts, Chem. Phys. 339(1–3) (2007) 64–72.

[3] T. Umebayashi, T. Yamaki, H. Itoh, K. Asai, Band gap narrowing of titanium dioxide by sulfur doping, Appl. Phys. Lett. 81 (2002) 454–456.

[4] W.-Y. Choi, A. Termin, The role of metal ion dopants in quantum-sized TiO_2: Correlation between photoreactivity and charge carrier recombination dynamics, J. Phys. Chem. 98(51) (1994) 13669–13679.

[5] R.L. Narayana, M. Matheswaran, A.A. Aziz, P. Saravanan, Photocatalytic decolourization of basic green dye by pure and Fe, Co doped TiO_2 under daylight illumination, Desalination 269(1–3) (2011) 249–253.

[6] T. Ohno, N. Murakami, T. Tsubota, H. Nishimura, Development of metal cation compound-loaded S-doped TiO_2 photocatalysts having a rutile phase under visible light, Appl. Catal., A 349(1–2) (2008) 70–75.

[7] X.-X. Yang, C.-D. Cao, L. Erickson, K. Hohn, R. Maghirang, K. Klabunde, Photo-catalytic degradation of Rhodamine B on C-, S-, N-, and Fe-doped TiO_2 under visible-light irradiation, Appl. Catal. B: Environ. 91(3–4) (2009) 657–662.

[8] Y.-R. Zhang, Q. Li, Synthesis and characterization of Fe-doped TiO_2 films by electrophoretic method and its photocatalytic activity toward methyl orange, Solid State Sci. 16 (2013) 16–20.

[9] D.V. Wellia, Q.C. Xu, M.A. Sk, K.H. Lim, T.M. Lim, T. Tan, Y. Tan, Experimental and theoretical studies of Fe-doped TiO_2 films prepared by peroxo sol–gel method, Appl. Catal., A 401(1–2) (2011) 98–105.

[10] P. Sathishkumar, S. Anandan, P. Maruthamuthu, T. Swaminathan, M.-F. Zhou, M. Ashokkumar, Synthesis of Fe^{3+} doped TiO_2 photocatalysts for the visible assisted degradation of an azo dye, Colloids Surf., A 375 (2011) 231–236.

[11] M. Adachi, Y. Murata, M. Harada, S. Yoshikawa, Formation of titania nanotubes with high photo-catalytic activity, Chem. Lett. 29 (2000) 942–943.

[12] S.Z. Chu, S. Inoue, K. Wada, D. Li, H. Haneda, S. Awatsu, Highly porous $(TiO_2–SiO_2–TeO_2)/Al_2O_3/TiO_2$ composite nanostructures on glass with enhanced photocatalysis fabricated by anodization and sol−gel process, J. Phys. Chem. B 107 (2003) 6586–6589.

[13] A. Michailowski, D. AlMawlawi, G.S. Cheng, M. Moskovits, Highly regular anatase nanotubule arrays fabricated in porous anodic templates, Chem. Phys. Lett. 349 (2001) 1–5.

[14] J.H. Jung, H. Kobayashi, K.J.C. van Bommel, S. Shinkai, T. Shimizu, Creation of novel helical ribbon and double-layered nanotube TiO_2 structures using an organogel template, Chem. Mater. 14 (2002) 1445–1447.

[15] S. Kobayashi, N. Hamasaki, M. Suzuki, M. Kimura, H. Shirai, K. Hanabusa, Preparation of helical transition-metal oxide tubes using organogelators as structure-directing agents, J. Am. Chem. Soc. 124 (2002) 6550–6551.

[16] Z.R. Tian, J.A. Voigt, J. Liu, B. Mckenzie, H.F. Xu, Large oriented arrays and continuous films of TiO_2-based nanotubes, J. Am. Chem. Soc. 125 (2003) 12384–12385.

[17] T. Kasuga, M. Hiramatsu, A. Hoson, T. Sekino, K. Niihara, Formation of titanium oxide nanotube, Langmuir 14 (1998) 3160–3163.

[18] Q. Chen, W.Z. Zhou, G.H. Du, L.H. Peng, Trititanate nanotubes made via a single alkali treatment, Adv. Mater. 14 (2002) 1208–1211.

[19] B.D. Yao, Y.F. Chan, X.Y. Zhang, W.F. Zhang, Z.Y. Yang, N. Wang, Formation mechanism of TiO_2 nanotubes, Appl. Phys. Lett. 82 (2003) 281–283.

[20] Q. Cai, M. Paulose, O.K. Varghese, C.A. Grimes, The effect of electrolyte composition on the fabrication of self-organized titanium oxide nanotube arrays by anodic oxidation, J. Mater. Res. 20 (2005) 230–236.

[21] C. Ruan, M. Paulose, O.K. Varghese, G.K. Mor, C.A. Grimes, Fabrication of highly ordered TiO_2 nanotube arrays using an organic electrolyte, J. Phys. Chem. B 109 (2005) 15754–15759.

[22] X. Quan, S. Yang, X. Ruan, H. Zhao, Preparation of titania nanotubes and their environmental applications as electrode, Environ. Sci. Technol. 39 (2005) 3770–3775.

[23] G.K. Mor, O.K. Varghese, M. Paulose, K. Shankar, C.A. Grimes, A review on highly ordered, vertically oriented TiO_2 nanotube arrays: Fabrication, material properties, and solar energy applications, Solar Energy Mater. Solar Cells 90 (2006) 2011–2075.

[24] L.G. Devi, R. Kavitha, A review on non metal ion doped titania for the photocatalytic degradation of organic pollutants under UV/solar light: Role of photogenerated charge carrier dynamics in enhancing the activity, Appl. Catal. B: Environ. 140–141 (2013) 559–587.

[25] S. Tieng, A. Kanaev, K. Chhor, New homogeneously doped Fe(III)–TiO_2 photocatalyst for gaseous pollutant degradation, Appl. Catal., A 399(1–2) (2011) 191–197.

[26] E.S. Elmolla, M. Chaudhuri, Photocatalytic degradation of amoxicillin, ampicillin and cloxacillin antibiotics in aqueous solution using UV/TiO_2 and UV/H_2O_2/TiO_2 photocatalysis, Desalination 252(1–3) (2010) 46–52.

[27] J.R. White, A.J. Bard, Electrochemical investigation of photocatalysis at cadmium sulfide suspensions in the presence of methylviologen, J. Phys. Chem. 89 (1985) 1947–1954.

[28] D.W. Bahnemann, J. Cunningham, M.A. Fox, E. Pelizzetti, P. Pichat, N. Serpone, in: R.G. Zepp, G.R. Heltz, D.G. Crosby (Eds.), Aquatic Surface Photochemistry, Lewis Publishers, Boca Raton, FL, 1994, p. 261.

[29] S. Kaur, V. Singh, TiO_2 mediated photocatalytic degradation studies of Reactive Red 198 by UV irradiation, J. Hazard. Mater. 141 (2007) 230–236.